ISSN 0021-3640, JETP Letters, 2012, Vol. 95, No. 11, pp. 555–559. © Pleiades Publishing, Inc., 2012.
Original Russian Text © N.S. Eliseeva, A.A. Kuzubov, S.G. Ovchinnikov, M.V. Serzhantova, F.N. Tomilin, A.S. Fedorov, 2012, published in Pis'ma v Zhurnal Eksperimental'noi i Teoreticheskoi Fiziki, 2012, Vol. 95, No. 11, pp. 633–637.

Theoretical Study of the Magnetic Properties of Ordered Vacancies in 2D Hexagonal Structures: Graphene, 2D-SiC, and h-BN

N. S. Eliseeva[a], A. A. Kuzubov[a–c], S. G. Ovchinnikov[a, c], M. V. Serzhantova[a, d, e, *], F. N. Tomilin[c], and A. S. Fedorov[c]

[a] *Siberian Federal University, Krasnoyarsk, 660028 Russia*
[b] *Siberian State Technological University, Krasnoyarsk, 660049 Russia*
[c] *Kirensky Institute of Physics, Siberian Branch, Russian Academy of Sciences, Akademgorodok, Krasnoyarsk, 660036 Russia*
[d] *Siberian State Aerospace University, Krasnoyarsk, 660014 Russia*
* *e-mail: sunrise.86@mail.ru*
[e] *Krasnoyarsk Branch, Moscow State University of Economics, Statistics, and Informatics, Krasnoyarsk, 660012 Russia*

Received April 17, 2012

The magnetic properties of vacancies in 2D hexagonal structures—graphene and 2D-SiC and h-BN monolayers—have been studied. It has been found that a local magnetic moment exists in all listed systems in the presence of vacancies. However, in 2D hexagonal silicon carbide, the local magnetic moment appears only in the presence of silicon vacancy. In addition, the effect of the distance between vacancies in a monolayer on transitions between the ferromagnetic and antiferromagnetic states has been revealed.

DOI: 10.1134/S0021364012110045

1. INTRODUCTION

Graphene is often used as a model system to study the properties of 2D compounds [1]. The fractional quantum Hall effect [2, 3], superconductivity [4], and some other quantum effects were described for graphene as an example of 2D structures. One of the important problems of condensed matter physics is correlation between the presence of conduction electrons in a system and its magnetic properties [5, 6]. The appearance of magnetic order in graphene was estimated as hardly possible because *d* and *f* electrons are absent in the carbon atom. This effect is explained by crystal [7–11] and structural defects [12]. It was shown in [13, 14] that point defects (vacancies) in graphene have local magnetic moments whose interaction with conduction electrons is responsible for the Kondo effect in the system [6, 15–17]. Chen et al. [13] believe that the modification of the graphene lattice by vacancies can lead to the implementation of magnetically ordered systems based on carbon nanostructures in which ferromagnet–antiferromagnet transitions are possible [18].

The appearance of the magnetic moment in the SiC monolayer, as well as in graphene, is due to vacancies. Spin-polarization calculations of vacancy defects in the SiC monolayer with the density functional theory and generalized gradient approximation were performed in [19], where it was shown that Si and C vacancies play different roles in the magnetism of the SiC monolayer. A silicon vacancy V_{Si} is responsible for the appearance of the local magnetic moment, whereas this moment is absent in a system with a carbon vacancy V_C. The absence of the magnetic moment in the 2D SiC monolayer with the carbon vacancy can be explained by structural distortions of the system. Since the atomic radius of silicon is larger than that for carbon, a weak bond can be formed between silicon atoms surrounding the carbon vacancy in 2D SiC, which leads to the formation of electron pairs. This effect is also characteristic of the 3C-SiC cubic crystal with carbon vacancies [20]. Spin-polarization calculations for the SiC monolayer with a single silicon vacancy [19] indicate that two configurations with the magnetic moments $4.0\mu_B$ and $1.9\mu_B$, which correspond to the high- and low-spin states, respectively, are possible in the system. The authors of that work found that the energy of the low-spin state is 0.039 eV lower than the energy of the high-spin state. Those calculations show that the spin density distribution in the low-spin state for the 2D SiC structure with one silicon vacancy is as follows: the spins of electrons in two and one of three carbon atoms surrounding the vacancy are upward and downward, respectively.

The h-BN monolayer with vacancies is another 2D structure where the magnetic moment appears [21–23], whereas spontaneous magnetization is absent in the absence of defects. The authors of [21] performed a density-functional study of six types of defects in the

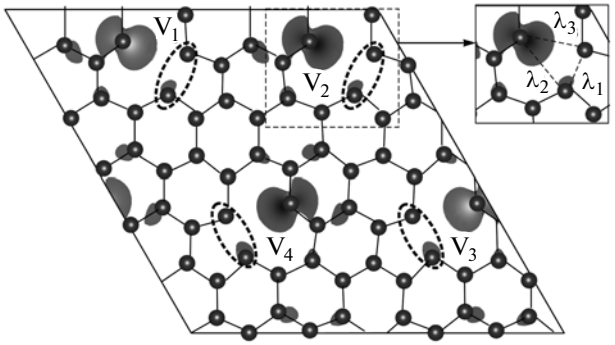

Fig. 1. Graphene supercell containing $6 \times 6 \times 1$ unit cells of graphene and four vacancies V_i; the dashed lines indicate the place of the dimerization of carbon atoms, and λ_i are the distances between atoms around vacancies.

structure of the h-BN monolayer: boron, V_N, and nitrogen, V_N, vacancies; the substitution of a nitrogen atom for boron B_N and vice versa N_B; and the substitution of the carbon atom for boron and nitrogen atoms C_B and C_N. The authors of [21] obtained spontaneous magnetization in the presence of substitutional impurities C_B and C_N or vacancies V_B and V_N in the h-BN structure. The calculated spin-polarization densities of states for C_B and C_N defects indicate the magnetization of the h-BN monolayer, which is $1.0\mu_B$ per defect. The system with V_B and V_N vacancies has spin polarization, which leads to the magnetic moments $3.0\mu_B$ and $1.0\mu_B$, respectively, because one and three unpaired electrons appear when a nitrogen atom and a boron atom are removed from the h-BN monolayer, respectively. The h-BN monolayer containing the B_N or N_B defect has no spin polarization.

According to the above presentation, the appearance of a single vacancy in graphene and 2D SiC and 2D h-BN monolayers can lead to the appearance of local magnetic moments. However, the existence of magnetic order in these structures with a high concentration of vacancies is still an open problem. In this work, the magnetic properties of vacancies in 2D hexagonal structures—graphene and 2D-SiC and h-BN monolayers—are studied. In particular, the effect of the distance between vacancies on a ferromagnet–antiferromagnet transition is analyzed.

2. OBJECTS OF INVESTIGATION AND CALCULATION METHOD

The calculations were performed with the density functional theory (DFT) [24] including the Perdew–Wang 91 (PW91) gradient corrections using the Vienna ab initio simulation package (VASP) [23–27] and the Vanderbilt ultrasoft pseudopotential [28].

In the first stage, graphene and 2D-SiC and h-BN monolayers without vacancies were calculated by simulating a hexagonal unit cell containing two atoms. Then, for graphene and 2D-SiC and h-BN monolayers, we considered three types of supercells with vacancies containing $6 \times 6 \times 1$ (68 atoms), $8 \times 8 \times 1$ (124 atoms), and $10 \times 10 \times 1$ (196 atoms) unit cells. Each simulated supercell included four vacancies. These supercells were chosen in order to satisfy the condition of the uniform distributions of vacancies. Structures with the uniform distribution of vacancies with different concentrations (table) were thus simulated. The program used in the calculations requires periodic conditions; for this reason, a vacuum gap of 15 Å was specified to simulate the monolayer along the normal to its plane. The vacuum gap was chosen under the assumption that the images of monolayers at this distance do not affect each other. The reciprocal space in the first Brillouin zone was automatically divided into a mesh according to the Monkhorst–Pack scheme [29]. The numbers of k points along each direction were $6 \times 6 \times 1$. The geometry optimization for each structure was performed to a minimum force of 0.01 eV/Å acting on an atom.

The ferromagnetic, antiferromagnetic, and nonmagnetic states were studied. The ferromagnetic state was obtained automatically in the spin-polarization calculation in the VASP. It implies the initial population of the system by electrons with the same directions of the spin projection. A low-spin state, which is energetically preferable [19], is obtained in this procedure for the 2D-SiC structure. The antiferromagnetic state in the compounds under study was specified by alternating magnetic moments on atoms surrounding a vacancy. In particular, the magnetic moments of atoms surrounding vacancies V_1 and V_3 in graphene (Fig. 1) were opposite to the magnetic moments of atoms surrounding vacancies V_2 and V_4. Similar ordering was used for 2D-SiC and h-BN monolayers. For comparison, a nonmagnetic state with zero total magnetic moment was calculated for each of the structures. It was found that the state calculated disregarding the magnetic interaction is energetically unfavorable for all systems under study. The results are summarized in the table, where $\Delta E_{\text{nonmag–mag}}$ is the energy difference between the most favorable magnetically ordered state (ferro- or antiferromagnetic) and the nonmagnetic state.

3. RESULTS AND DISCUSSION

The calculations show that the nonmagnetic state is energetically unfavorable for all compounds under study (see table).

Graphene with vacancies exhibits the following feature. Two of three carbon atoms surrounding a vacancy approach each other with the appearance of a weak bond (dimerization), forming five-member structures (see Fig. 1). A similar result for a single vacancy was obtained in [18]. Atoms surrounding the

Characteristics of magnetic order in 2D hexagonal structures: graphene and 2D-SiC and h-BN monolayers

Compound	C, %	R, Å	S_{aver}, μ_B	ΔE_{F-AF}, eV	$\Delta E_{nonmag-mag}$, eV
Graphene with vacancies	5.56	7.4	1.4	0.0064	1.5642
	3.13	9.8	1.1	0.0047	1.7977
	2.00	12.2	1.1	–0.0146	1.5556
2D-SiC monolayer with silicon vacancies	5.56	9.2	1.6	0.0543	0.6800
	3.13	12.3	1.6	–0.0592	1.3297
	2.00	15.4	1.5	0.0022	1.5353
h-BN monolayer with boron vacancies	5.56	7.5	1.7	0.3378	0.1394
	3.13	10.0	2.2	–0.0670	0.9843
	2.00	12.5	2.3	–0.0323	1.1834
h-BN monolayer with nitrogen vacancies	5.56	7.5	0.9	–0.0079	0.2174
	3.13	10.0	0.9	0.0080	0.2570
	2.00	12.5	0.9	0.0007	0.2882

vacancy form a triangle for all types of supercells ($6 \times 6 \times 1$, $8 \times 8 \times 1$, and $10 \times 10 \times 1$). In particular, this triangle for the graphene supercell containing $6 \times 6 \times 1$ unit cells has the sizes $\lambda_1 = 1.81$ Å, $\lambda_2 = 2.62$ Å, and $\lambda_3 = 2.79$ Å. Then, the spin density distribution in the supercell was simulated (Fig. 1). It is seen that magnetic moments are localized only on those carbon atoms surrounding vacancies that do not enter into dimerized pairs. In all figures, the gray regions mark the localization of the spin density, which was calculated by the formula

$$\rho_s = \rho_\alpha - \rho_\beta,$$

where ρ_α and ρ_β are the density distribution of spin-up and spin-down electrons, respectively. The different colors correspond to different signs of the spin density.

The calculations for graphene with vacancies indicate that, with an increase in the supercell (i.e., with an increase in the distance between vacancies), a transition from the antiferromagnetic to ferromagnetic order was observed. The results are presented in the table, where ΔE_{F-AF} is the energy difference between the ferromagnetic and antiferromagnetic states. The positive and negative values of this quantity indicate that the antiferromagnetic and ferromagnetic states are favorable.

The distribution of the magnetic moment in the 2D-SiC monolayer with silicon vacancies is more complex. The spin density is localized on carbon atoms surrounding a silicon vacancy and forming an equilateral triangle (first coordination sphere of the interaction between the magnetic moments of vacancies). The spin projections of two of three atoms sur-

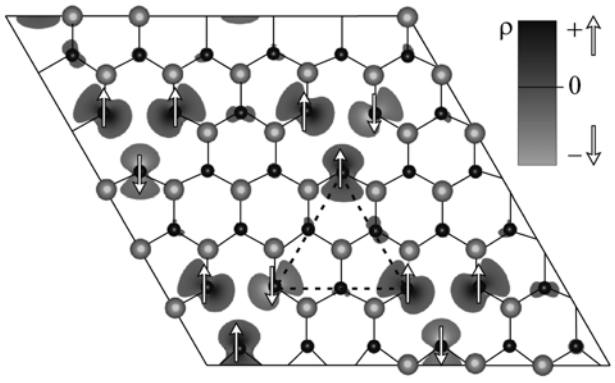

Fig. 2. Localization of magnetic moments for the ferromagnetic state of 2D-SiC; black and gray colors mark carbon and silicon atoms, respectively; and the dashed triangle shows the second coordination sphere of the interaction between vacancies.

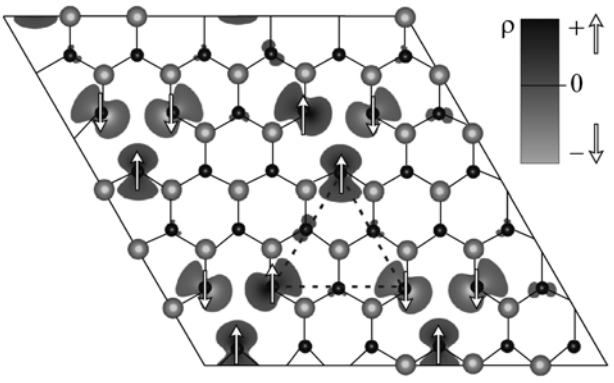

Fig. 3. Localization of magnetic moments for the antiferromagnetic state of 2D-SiC; black and gray colors mark carbon and silicon atoms, respectively; and the dashed triangle shows the second coordination sphere of the interaction between vacancies.

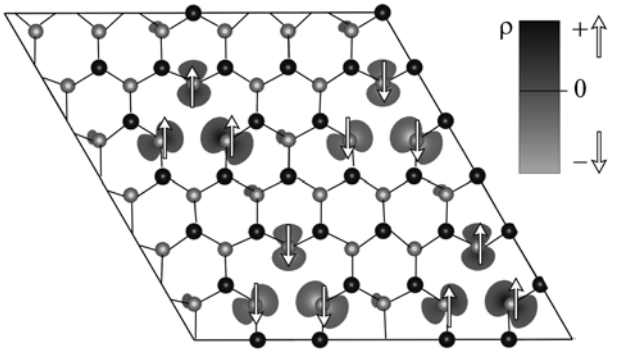

Fig. 4. Localization of magnetic moments for the antiferromagnetic state of the h-BN monolayer with nitrogen vacancies; dark and gray circles are nitrogen and boron atoms, respectively.

rounding the vacancy have the same direction opposite to the spin projection of the third atom (Figs. 2 and 3). For the ferromagnetic and antiferromagnetic states, we considered various combinations of the directions of the magnetic moments on neighboring vacancies. The energy difference between the configurations is no more than 0.2 eV. The most favorable configuration for both ferromagnet and antiferromagnet depends on the distribution of the unpaired electrons on neighboring vacancies (the second coordination sphere of the interaction between the magnetic moments of vacancies is shown in Figs. 2 and 3 by a dashed line). Vacancies of the second coordination sphere form a triangle. The directions of the spin projections of electrons on two of the vacancies are the same and opposite to the spin projection of the electron on the third vacancy.

Ferromagnetic and antiferromagnetic orderings in the 2D-SiC monolayer with silicon vacancies, as well as in graphene, depend on the distance between vacancies (see table). In this case, there are one ferromagnetic and two antiferromagnetic states.

No magnetic moment in the system with the carbon vacancy is present. A similar result for a single vacancy was obtained in [19].

The magnetic moment in h-BN monolayers appears in the presence of both boron and nitrogen vacancies. In both cases, atoms surrounding a vacancy are equidistant from each other; i.e., dimerization is not observed. The spin density is uniformly distributed over the atoms surrounding the vacancy. The spin projections on these atoms are codirected (see Fig. 4).

As the distance between boron vacancies increases, a transition from the antiferromagnetic to ferromagnetic order is observed. The situation for nitrogen vacancies is opposite: a transition from the ferromagnetic to antiferromagnetic order occurs.

4. CONCLUSIONS

The theoretical studies have demonstrated that the presence of vacancies in 2D hexagonal structures—graphene and 2D-SiC and h-BN monolayers—leads to the appearance of a magnetic moment, except for the case of silicon carbide with a carbon vacancy. It has been shown that magnetically ordered states appear in the systems under study at high concentrations of vacancies. An increase in the distance between vacancies can be accompanied by a transition from the antiferromagnetic to ferromagnetic state and vice versa, depending on the type of vacancies. The discovery of this phenomenon opens prospects for using vacancies in graphene and 2D-SiC and h-BN monolayers to induce and control a magnetic order.

We are grateful to the Institute of Computational Modeling, Siberian Branch, Russian Academy of Sciences (Krasnoyarsk); the Joint Supercomputer Center, Russian Academy of Sciences (Moscow); and the Complex of High-Productivity Calculations, Institute of Space and Information Technologies, Siberian Federal University (Krasnoyarsk), for the opportunity of using their computer clusters to perform the calculations.

REFERENCES

1. A. K. Geim, Science **324**, 1530 (2009).
2. K. I. Bolotin, F. Ghahari, M. D. Shulman, et al., Nature **462**, 196 (2009).
3. X. Du, I. Skachko, F. Duerr, et al., Nature **462**, 192 (2009).
4. H. B. Heersche, P. Jarillo-Herrero, Oostinga, et al., Nature **446**, 56 (2007).
5. P. W. Anderson, Phys. Rev. **124**, 41 (1961).
6. J. Kondo, Prog. Theor. Phys. **32**, 37 (1964).
7. J. Cervenka, M. I. Katsnelson, and C. F. J. Flipse, Nature Phys. **5**, 840 (2009).
8. P. Esquinazi, D. Spemann, R. Höhne, et al., Phys. Rev. Lett. **91**, 227201 (2003).
9. M. M. Ugeda, I. Brihuega, F. Guinea, et al., Phys. Rev. Lett. **104**, 096804 (2010).
10. P. O. Lehtinen, A. S. Foster, Y. Ma, et al., Phys. Rev. Lett. **93**, 187202 (2004).
11. M. Fujita, K. Wakabayashi, K. Nakada, et al., J. Phys. Soc. Jpn. **65**, 1920 (1996).
12. N. Park, M. Yoon, S. Berber, et al., Phys. Rev. Lett. **91**, 237204 (2003).
13. J.-H. Chen, L. Li, W. G. Cullen, et al., Nature Phys. **7**, 535 (2011).
14. J.-H. Chen, W. G. Cullen, C. Jang, et al., Phys. Rev. Lett. **102**, 236805 (2009).
15. K. Sengupta and G. Baskaran, Phys. Rev. B **77**, 045417 (2008).
16. P. S. Cornaglia, G. Usaj, and C. A. Balseiro, Rev. Lett. **102**, 046801 (2009).
17. M. Hentschel and F. Guinea, Phys. Rev. B **76**, 115407 (2007).

18. O. V. Yazyev and L. Helm, Phys. Rev. B **75**, 125408 (2007).
19. X. He, T. He, Zh. Wang, and M. Zhao, Physica E **42**, 2451 (2010).
20. A. Zywietz, J. Furthmuller, and F. Bechstedt, Phys. Rev. B **62**, 6854 (2000).
21. S. Azevedo, J. R. Kaschny, C. M. C de Castilho, and F. de Brito Mota, Eur. Phys. J. B **67**, 507 (2009).
22. M. V. Serzhantova, A. A. Kuzubov, A. S. Fedorov, et al., J. Exp. Theor. Phys. **112**, 664 (2011).
23. A. A. Kuzubov, M. V. Serzhantova, A. S. Fedorov, et al., JETP Lett. **93**, 335 (2011).
24. W. Kohn and L. J. Sham, Phys. Rev. B **140**, 1133 (1965).
25. G. Kresse and J. Hafner, Phys. Rev. B **47**, 558 (1993).
26. G. Kresse and J. Hafner, Phys. Rev. B **48**, 13115 (1993).
27. G. Kresse and J. Hafner, Phys. Rev. B **49**, 14251 (1994).
28. D. Vanderbilt, Phys. Rev. B **41**, 7892 (1990).
29. H. J. Monkhorst and J. D. Pack, Phys. Rev. B **13**, 5188 (1976).

Translated by R. Tyapaev